Experimental investigation of phase change of medium/high temperature paraffin wax embedded in 3D periodic structure

Giulia Righetti[a], Luca Doretti[b], Claudio Zilio[a], Giovanni A. Longo[a], Simone Mancin[a,*]

[a] *Department of Management and Engineering, University of Padova, Vicenza, 36100, Italy*
[b] *Department of Civil, Environmental and Architectural Engineering University of Padova, Padova, 35131, Italy*

ARTICLE INFO

ABSTRACT

In the scientific and industrial community, the interest on Latent Thermal Energy Storages (LTESs) is continuously increasing. These components can be easily coupled with intermittent renewable energy sources and with heat sources that undergo to cycling operations. Phase Change Materials (PCMs) are considered convenient and reliable media to be used in LTES. Nevertheless, their low thermal conductivity remains the greatest hindrance that still limits their technological application. The present work aims at increasing the effective thermal conductivity of a paraffin wax, the RT70, having a phase change temperature of 70 °C. This paper proposes the addition of a 3D metallic periodic structure to the PCM. To optimize the geometry, three different structures with 10, 20, and 40 mm base sizes were designed and manufactured via additive manufacturing. Experimental tests were run during the melting and the solidification of RT70 at three different heat fluxes (10, 20, and 30 W). The addition of the 3D aluminum structure in the PCM remarkably improved the heat transfer performance as compared to the reference empty box. The best geometry was identified, and a correlation was proposed to evaluate the charging time.

INTRODUCTION

As reported by recent review papers [1, 5, 7, 15], in the last years, several studies have been published on PCMs and on how they can be efficiently applied to LTESs. In fact, thanks to their phase change process, they can provide higher energy density during the melting and the solidification processes with respect to the standard sensible heat storages. Therefore, PCM based LTES can be more compact while storing the same amount of energy as compared to a standard sensible TES. However, in order to design an efficient LTES, a proper and effective PCM is required. The ideal one should be chemically stable, nontoxic, non-corrosive and cheap. Furthermore, its phase change temperature should be congruent with the future operations and the subcooling as small as possible [24]. Obviously, its latent heat of fusion and thermal conductivity should be as large as possible while the volume expansion during the melting as lower as possible.

Currently, several materials with a wide range of phase change temperatures (i.e., from −20 °C to +200 °C) are available as PCMs. Among them, there is the large group of paraffin waxes. They are very widespread thanks to many desirable characteristics: high latent heat, chemical inertia, non-toxicity, stability, among others. However, it is also well-known that they present a relatively low thermal conductivity, that substantially penalizes the LTES efficiency and still limits their commercial deployment.

At the current state of the art, several techniques to enhance the thermal conductivity have already been proposed, well resumed in the review papers by Al-Maghalseh and Mahkamov (2019), Mahdi et al. [8], Tao et al. [21], Tauseef-ur-Rehman et al. [16]. Nevertheless, Mahdi et al. [8] stated that the work already done in this field is insufficient and recommended to further investigate the application of extended surfaces coupled to PCM in order to define a cost effective and efficient heat transfer intensification technique.

In the open literature, some researchers proposed the addition of metal structures to the PCM, especially as fin type structures.

Ismail and Lino [4] investigated the use of radial fins and turbulence promoters located inside a horizontal tube filled with PCM and they concluded that there is an ideal fin diameter that increases the interface velocity and decreases the solidification time. Hosseinizadeh et al. [3] also studied the fin effect on the PCM heat transfer performances by varying the fin geometry. Higher values of fin number and height promoted the overall heat transfer, while the results had only a weak sensitivity on fin thickness. The Authors finally suggested the optimum fin parameters, above which the heat sink performance showed no further improvement. Mahmoud et al. [9] investigated different options to increase the thermal conductivity: the addition

* Corresponding author: Prof. Simone Mancin, Department of Management and Engineering, University of Padova, Str.lla S. Nicola 3, Vicenza 36100, Italy. pH: +39-0444-998746.
E-mail address: simone.mancin@unipd.it (S. Mancin).

Nomenclature

c_p	specific heat (J kg^{-1} K^{-1})
Fo	Fourier number (-)
I	electric current (A)
k	coverage factor (-)
P_{EL}	electric power (W)
q_{eff}	effective heat flow rate (W)
q_{loss}	loss heat flow rate (W)
r	latent heat (J kg^{-1})
Ste	Stefan number (-)
t	temperature (°C)
x	position (m)
ΔV	voltage (V)

Greek letters

ε	porosity (-)
Θ	non-dimensional temperature (-)
λ	thermal conductivity (W m^{-1} K^{-1})
ρ	density (kg m^{-3})

Subscripts

COM	composite
EMM	expanded metal mesh
exp	experimental data
i	initial
j	junction
LTES	latent heat thermal energy storage
melt	melting
PCM	phase change material
S	solid
sim	simulated data

of cross fins, of parallel fins and of a honeycomb structure. Experimental results have shown that the heat transfer improves with the use of these structures, especially if the number of fins is increased (i.e. fin spacing decreased). Furthermore, similar results could be obtained by using the honeycomb insert with costs and weight reduction. Mustaffar et al. [12] studied the PCM behavior when embedded in an expanded metal mesh composed of five 160 × 114 × 9 mm aluminum rectangular layers displayed in perpendicular and parallel way having a porosity of about 89%. This particular structure improved the PCM thermal conductivity and consequently reduced the phase change time of about 14%. Shuja et al. [19] proposed to insert aluminum meshes having different shapes (rectangular, triangular, and hexagonal) in a PCM to increase its heat transfer performance. The Authors concluded that the triangular geometry outperformed the others, since it presented a shorter phase change time and an earlier melting starting point. Kamkari and Groulx [6] studied the addition of fins at different inclination angles to some rectangular enclosures filled of PCM. The experiments demonstrated that the phase change process is dominated by heat conduction and that the melting rate is accelerated by the decrement of the inclination angle and by the addition of fins to the vertical enclosure.

Furthermore, it is well-known that the operating temperature is one of the most dominant factors affecting performance, lifespan and safety of electronics. Nevertheless, in the open literature there are still few and very recent papers dealing with relatively high phase change temperature PCMs [14, 20, 22, 23] coupled with LTESs. Such structures are going to be efficiently applied also to high-temperature and largely widespread purposes, such as Lithium-ion batteries, electronics, transformers, antennas, etc., so proper PCMs should be tested.

The present paper proposes an experimental optimization of a PCM based heat storage to improve the thermal management of constant heat flux devices. Given the melting temperature, i.e. 70 °C of the selected PCM, this study focuses on medium/high temperature applications. The investigated samples were of relatively small dimensions, but, thanks to their symmetry, they could also be seen as elements of larger modular systems.

As reported in Righetti et al. [18], the present authors carried out a study to investigate a potential solution to increase the efficiency of latent thermal energy systems based on low thermal conductivity PCMs. The proposed idea was to insert some aluminum structured ligaments inside the PCM, to spread the heat more homogeneously inside the storage system.

Among the infinite possible geometries, a 3D periodic structure based on a pyramidal cell was selected because of its simplicity and replicability. The periodicity and the symmetry of these peculiar structures allowed for the creation of a great number of customized geometries. In this way, the pore size effect could be isolated and studied, while keeping constant the porosity.

The results published in Righetti et al. [18] showed that it is possible to reduce charging and discharging times using optimized 3D structures, and the pore size affects the performance of the LTES. An optimized 3D structures can guarantee faster and efficient energy storage and release, leading to a more homogeneous temperature distribution in the PCM. Finally, the use of aluminum structures has led to a lower junction temperature. All these positive characteristics have led to believe that the use of 3D structures might be a suitable solution to overcome the low thermal conductivity issue, typical of almost all the available PCMs.

In this paper the focus has been moved to a different PCM. In fact, from an analysis of the literature it has been noted that few data are available for paraffin waxes having a medium-high phase change temperature. Furthermore, it is very important and it is not obvious to know whether or not comparable results can be obtained with two similar PCMs (i.e. paraffin waxes), having different melting temperature. For these reasons, another paraffin wax presenting a melting temperature of 70 °C was selected and tested, the RT70.

The tests were subdivided in charging and discharging phases. During the charging phase, the sample was heated by an electric resistance by varying the heat fluxes between 5 and 16 kW m^{-2}. The temperature fields in the paraffin, in the 3D structure, and in the basement were monitored and recorded while several videos were recorded to better understand the phase change processes.

In order to be able to compare the results with those already obtained for RT55, the same geometries proposed in Righetti et al. [18] were used. They have three different base sizes: 10 mm, 20 mm, and 40 mm. The porosity was kept equal to 0.95 to isolate and focus on the base size (i.e. pore size) influence on the phase change process. The collected experimental measurements contribute to build a robust and reliable database of the performance of PCMs, which is undoubtedly needed to improve the understanding of the heat transfer mechanisms during the solid-liquid phase change. Furthermore, the model presented in Righetti et al. [18], which was validated only on the RT55 data, was successfully implemented to estimate the results collected for RT70.

EXPERIMENTAL materials and METHODS

Test samples

This work aims at comparing the performance of three different 3D periodic geometries when applied to PCM latent thermal energy storages, hence, three samples with periodic structures and an empty reference sample were manufactured via additive manufacturing. The AlSi10Mg-0403 aluminum alloy was used due to its favorable properties in the current 3D printing technologies.

The thermal diffusivity of this alloy was experimentally measured with a Transient Hot Disk TPS 2500S instrument (maximum uncertainty ($k = 2$) lower than $\pm 5.0\%$ of the reading) at ambient temperature of 20 °C. The average value of 10 measurements was equal to 41.57 mm^2 s^{-1}. So, the thermal conductivity was estimated to be around 96 W m^{-1} K^{-1}. This value is pretty low for an aluminum alloy, but one has to consider that the samples were obtained via additive manufacturing, so the presence of porosity is almost unavoidable as compared to other manufacturing processes.

A schematic and a picture of three samples containing the three different 3D structures and of the reference one are reported in Fig. 1, while the main geometrical characteristics are listed in Table 1.

The samples have square base of 0.042×0.042 m and a height of 0.06 m; they present a 0.012 m thick base of bulk 3D printed aluminum to homogenize the imposed heat flux. A 1 mm hole was drilled 0.5 mm below the surface to host a thermocouple to measure the temperature. The remaining 0.048 m height over the thick base is empty in the reference specimen or it presents the 3D structure, which is 0.04 m high. The last 8 mm on the top of the structure are used to permit the material expansion during the melting process. For further details, the reader can find out all the geometrical characteristics of the samples in Fig. 1 and Table 1. As described before, this paper investigates three different periodic structures all based on a pyramidal cell shape. Three cell base dimensions were studied: 10 mm, 20 mm, and 40 mm. For this reason, the specimens will be called 10 mm, 20 mm, and 40 mm, respectively.

All the samples present the same porosity, defined as the ratio between the volume of void and the total volume, equal to 95%, so that the structures present ligaments with different diameters (see Fig. 1a).

Table 1
Main geometrical characteristics of the 3D structured materials.

Parameter	Reference	10 mm	20 mm	40 mm
Base width			42 mm	
Base length			42 mm	
Total height			48 mm	
3D structure height	–		40 mm	
3D cell base size	–	10 mm	20 mm	40 mm
Ligament diameter	–	1 mm	2 mm	4 mm

PCM characteristics

As briefly discussed in the introduction, paraffin waxes are one of the most common PCMs, since they present several favorable properties. The paraffin wax selected in this work presents a melting temperature of around 70 °C, it was acquired from RUBITHERM®, and its commercial name is RT70.

The main thermo-physical characteristics, as declared by the manufacturer, are listed in Table 2. The same Table 2 also presents the main properties of another paraffin wax, named RT55, which was used to run a comparison with the results collected for the RT70. All the samples were filled with 50±0.1 g of the selected paraffin waxes.

Experimental setup

The test rig used in these experiments is presented in Fig. 2. It was designed to melt the PCM inside samples by means of an electric resistance and to monitor the temperature field during melting and solidification.
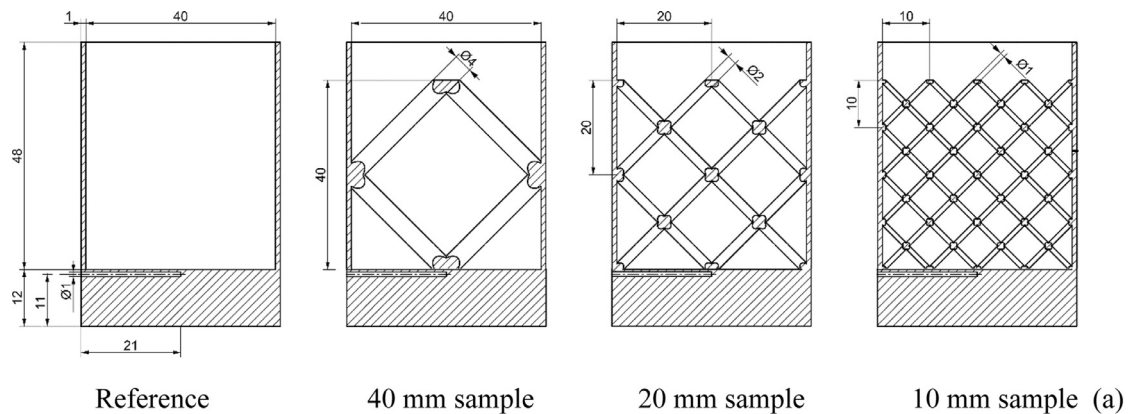

Reference   40 mm sample   20 mm sample   10 mm sample (a)

(b)

Fig. 1. Drawings (a) and a picture (b) of the four investigated samples.

Table 2
Paraffin RUBITHERM® RT70 and RT55 main thermophysical properties.

	RT70	RT55	
Melting area	69−71 main peak 70 °C	5 1−57 main peak 55 °C	°C
Congealing area	71−69 main peak 70 °C	5 5−57 main peak 55 °C	°C
Heat storage capacity ±7.5%	260 temp. range: 62−77 °C	170 temp. range: 48 - 63 °C	kJ kg^{-1}
Specific heat capacity	2	2	kJ kg^{-1} K^{-1}
Solid density at 15 °C	880	880	kg m^{-3}
Liquid density at 80 °C	770	770	kg m^{-3}
Heat conductivity (both phases)	0.2	0.2	W m^{-1} K^{-1}
Volume expansion	12	14	%
Flash point (PCM)	227	> 200	°C
Max. operation temperature	110	9 0	°C

Two main components can be identified: the 3D printed sample and a heater block that hosts in its center an 8 mm diameter 200 W/ 240 V electric cartridge heater controlled by a Variac transformer. The heater block is a 0.042 × 0.042 × 0.02 m aluminum plate having a thermal conductivity of 205 W m^{-1} K^{-1}. It is coupled with the sample with a silicone heat transfer paste with a thermal conductivity of 5 W m^{-1} K^{-1}. The heater is located in an insulated basement structure made of wood and filled up with rock wool to limit as much as possible the heat losses to the surroundings.

The heat flow rate generated by the heater can be evaluated by the Ohm's Law (Eq. (1)):

$$P_{EL} = \Delta V \cdot I \tag{1}$$

Where I is the current measured by a shunt resistance, equal to 0.0025 Ω ±0.25% at 25 °C; ΔV is the voltage variation at the heater. The uncertainty of the electrical power measurement was always estimated to be less than ±0.5%.
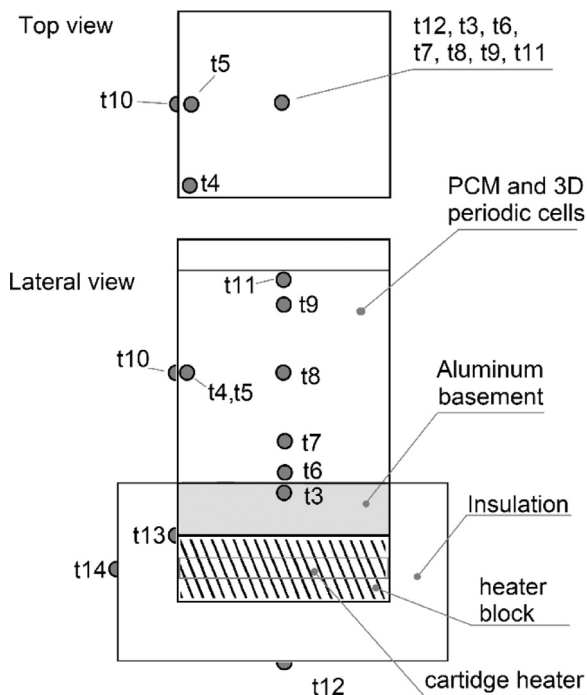

Fig. 2. Scheme of the experimental test rig and of the thermocouple locations.

The experimental tests were run in a climatic room with a temperature stability of ±0.2 °C. Several repeatability tests were done by repeating five times the same testing condition. Mismatches always below ±4% on the total charging time, and below ±3% on the total discharging time were observed, accordingly.

Furthermore, several T-type thermocouples (±0.1 °C) were implemented to monitor and record the temperature field inside the PCM and in some other meaningful locations. All the temperature values were recorded at 1 Hz by a 34970A Agilent Data Acquisition System and processed by a LabView software.

As it can be seen in Fig. 2, the following temperature measurements were accomplished:

- a thermocouple named t3 was inserted in the bulk 3D printed basement, just 0.5 mm below the PCM surface. It is called "junction temperature" and it might also be considered representative of the temperature of a potential electronic device that is going to be cooled by the LTES;
- six thermocouples named from t4 to t9 were inserted in the PCM thanks to a rigid structure hanged on the top of the sample. More in detail: t4 was located close to a corner, t5 close to a lateral wall, t6, t7, t8, and t9 in the center of the base sample at 1 mm, 5 mm, 20 mm, and 35 mm, respectively, from the basement;
- a thermocouple named t10 was attached on the external lateral wall in correspondence with the t5 thermocouple;
- a thermocouple named t11 was attached on the central highest vertex of the aluminum structure. In the reference sample, this thermocouple was not implemented;
- three other thermocouples, named t12, t13, and t14, were positioned in the insulated structure to monitor the heat losses to the environment and to calibrate the numerical simulation to accurately evaluate them.

The samples were heated with an electric resistance inserted in the basement and the associated heat flow rate P_{EL} was measured and evaluated using Eq. (1). However, the effective heat flux q_{eff} supplied to the samples depends also on the unavoidable heat losses to the surroundings q_{loss} as presented in Eq. (2).

$$q_{eff} = P_{EL} - q_{loss} \tag{2}$$

In order to estimate the heat losses, an original combined experimental-numerical approach was followed as proposed by Patankar et al. [13]. The complete description of the procedure can be found in Righetti et al. [18]. The first step consisted of a dedicated experimental test campaign on an aluminum block with the same dimensions as the investigated samples: 42 × 42 × 60 mm, which was equipped with several T-type thermocouples and coupled to the heater block using the same amount of the silicon thermal paste. The tests allowed to measure the steady state temperature distribution in the aluminum block, in the heater block and insulation and on the faces of the entire system that were exposed to the ambient, at different imposed electrical power. The heat flux was increased until the aluminum temperature reached a maximum mean temperature of around 115 °C. The second step of the procedure was to realize a numerical model of the setup and run an iterative procedure to estimate the heat transfer coefficients on the side surface of the aluminum block and insulation while the measured value of the heat flux was imposed.

A constant heat flux applied at the heater block and convection heat transfer coefficients on each external surface were applied as model boundary conditions. A grid sensitivity analysis was carried out and the results were found to be independent for a number of cells greater than ~300,000. The primary objective of the numerical model is to predict the natural convection boundary conditions and overall heat losses that cannot be determined directly from the available experimental data. Thus, for each calibration data point, the free variables in the numerical simulation are the convective heat transfer coefficients on the side surface of the aluminum block and insulation.

When all the measured experimental temperatures were matched within ± 0.1 K, the procedure ended and the heat losses were calculated by subtracting from the imposed heat flow rate, the one that is exchanged by natural convection through the side walls.

The results revealed that the heat losses can be estimated by:

$$|q_{loss}| = 0.0162 \times -t[°C] - 0.3459[W] \qquad (3)$$

The described procedure allowed to estimate both the convective heat transfer coefficient between the hot surface and the ambient and the heat loss; thus, to further confirm the described procedure, an additional calibration test was carried out. In particular, for each investigated electrical power, some dedicated experiments were run in the same test rig by using the reference sample (i.e. the empty box), which was filled with distilled water (64 g) and then heated from 20 °C up to 90 °C. A cover plate was positioned on the top of the sample to limit the water evaporation when the temperature went above the 70 °C. During the tests, the water temperature field was recorded by means of six thermocouples, named from t4 to t9, whom locations are illustrated in Fig. 2. A parallel numerical simulation was run using Ansys Fluent 18.2. The estimated values of convective heat transfer coefficients and heat losses were imposed as boundary conditions as well as the specific heat flux of each test. Fig. 3 presents the comparison between experimental and calculated average water temperatures for each heat flux: an excellent agreement was achieved. This confirmed that the adopted combined experimental-numerical calibration procedure represents a robust method to estimate the heat losses in this kind of experimental setups.

Test campaign methodology

In this experimental work, the complete PCM charging and discharging phases inside four samples are investigated. The charging process was analyzed under three different imposed electrical powers, 10 W, 20 W, and 30 W. It starts when the entire sample is isothermal at the ambient temperature and it finishes when the paraffin is fully melted. Then, the heating resistance is switched off and the discharging phase can start. It ends when the sample reaches 25 °C by exchanging heat via natural convection to the still ambient air. The sample was kept for the whole test duration inside a climatic chamber set at 20 °C.

The temperature inside the PCM was continuously monitored since it indicates the thermal performance of the sample. Results are commented in terms of temperature distribution and charging and discharging times.

Results

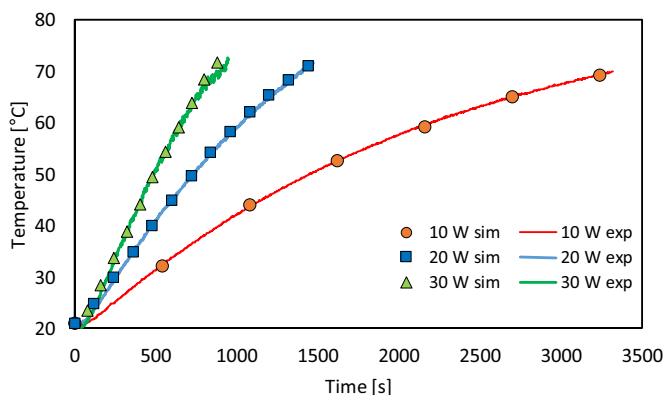In what it follows, the experimental results are presented and discussed. They are subdivided into two sections: the first refers to the charging phase while the second presents the discharging one. In each section, the total phase change times are compared among the samples, then some images taken from the videos (available as supplementary data) recorded during the experimental tests are reported and commented, finally the temperature field inside the PCM is discussed.

Charging phase

Table 3 resumes the charging times of all the specimens at the three investigated heat fluxes. For the sake of clarity, the second part of Table 3 reports the percentage reduction in charging time when the 3D structures are used with respect to the reference one.

More in detail, Fig. 4 presents the temperature measured by the thermocouple t8 located in the center of the PCM during the melting phase for each test: Fig. 4a reports the 30 W tests, Fig. 4b the 20 W tests and Fig. 4c the 10 W tests.

The use of each 3D periodic structure allows for a remarkable reduction of the charging time. In fact, the aluminum ligaments increase the heat transfer area, since they are directly connected to the heated basement, and efficiently spread the heat throughout the paraffin wax. In fact, conduction is the major heat transfer mechanism between PCM and the heater, as also observed and stated by Biwole et al. (2018) and Kamkari and Groulx [6].

The charging time reduction increases with an increase of the applied heat flux. On average, the time is 4.5% shorter when 10 W are imposed, but the reduction is on average 13.8% in the 30 W tests. This may be explained considering that the enhancement due to the metallic ligaments is much more effective at high heat fluxes because the amount of heat to be dissipated is greater and the metallic structure allows for an efficient heat spreading throughout the PCM. At the contrary, in the case of the empty box, the heat has to be conveyed through the PCM that acts as an insulator rather than as a heat transfer medium and thus the melting time and the PCM superheating are greater.

On the basis of the present results, the most efficient structure appears to be the 10 mm one. In fact, it allows for more significant time reductions as compared to the others (up to 17.2%, see Table 3). Similar results were also found by Righetti et al. [18] for a different PCM, RT55. Besides, since the time reduction increases with the decreasing of the base size, a sample having an even smaller base size (for instance 5 mm or so) should be even more efficient than the 10 mm. Nevertheless, as found by Mancin et al. [11] and Righetti et al. [17] for stochastic porous structures, for cell size equal or smaller than around 5 mm, there is not any noticeable difference in the exhibited enhancement.

By analyzing Fig. 4, it can be seen that the reference sample reaches higher final temperatures. In fact, it required a longer time to

Fig. 3. Water tests: comparison between experimental and numerical results.

Table 3
Charging times and percentage reduction in charging time when the 3D structures are used with respect to the reference sample.

	Reference [min]	10 mm [min]	20mm [min]	40 mm [min]
10 W	112	106	107	108
20 W	43	37	38	39
30 W	29	24	25	26

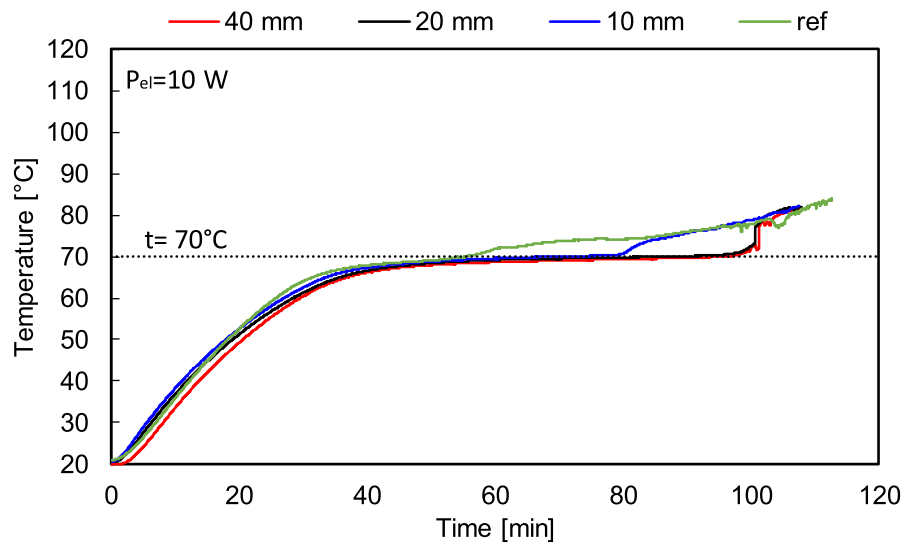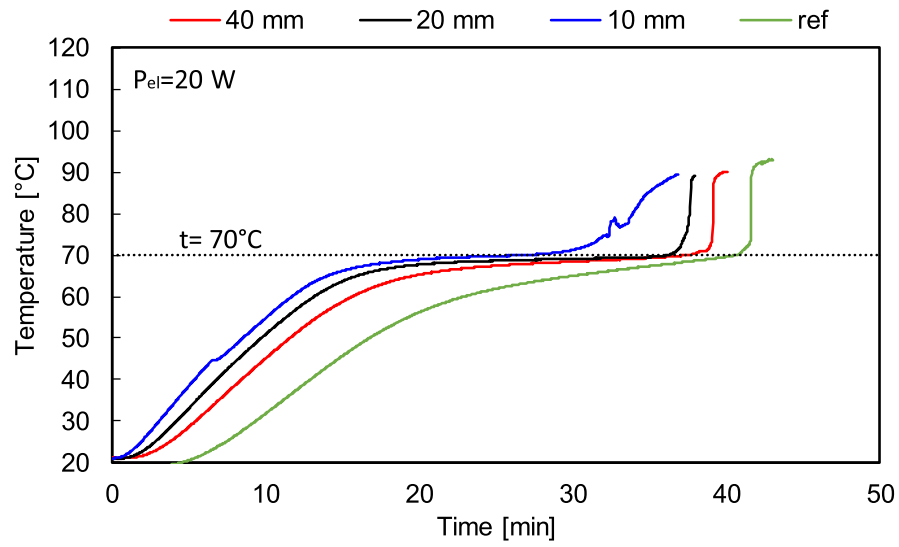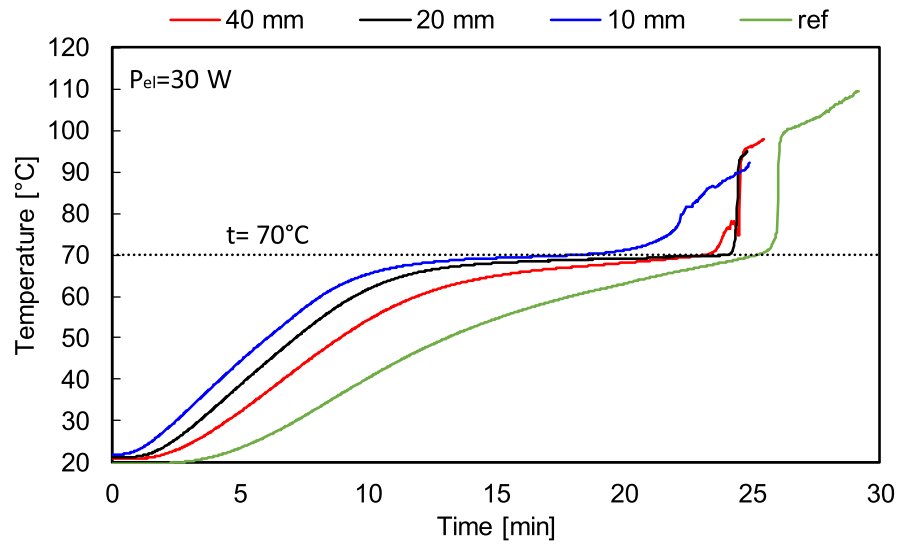| Percentage reduction with respect to the reference(%)				
	Reference	10 mm	20mm	40 mm
10 W	–	−5.4	−4.5	−3.6
20 W	–	−14.0	−11.6	−9.3
30 W	–	−17.2	−13.8	−10.3

Fig. 4. Temperature in the center of the PCM (t8) during RT70 charging phase at 30 W (a), 20 W (b), and 10 W (c) in the 40 mm, 20 mm, 10 mm samples and in the reference one.

totally melt the PCM due to its low average thermal conductivity. For this reason, in certain areas the liquid paraffin wax is strongly superheated, so the final temperature is higher than in the other structures.

At the beginning of the test during the sensible heating before the melting point, the temperature in the core increases for all the samples with a similar trend. Then, during the phase change, the temperature slope decreases and the 10 mm sample seems to take a shorter time to complete the melting process. This can be explained considering that in the case of 10 mm structure, the temperature of the core is on average slightly higher as compared to those of the other samples (see for instance the data taken at 30 W, Fig. 4a). This allows for a faster melting process. Close to the end of the charging phase, t8 rapidly increases: in this moment, hot liquid wets in the thermocouple and the melting front moves upward. Then a few minutes later, all the PCM is melted.

At an imposed heat flow rate of 10 W (Fig. 4c), the three enhanced samples show almost the same profiles, this can be due to the fact that the power is so low that even the conduction through the structure cannot significantly improve the performance.

Moreover, the core temperature in the reference sample increases faster than those measured in the others, this is probably due to a different distribution of the liquid during the melting process.

To better understand the underlying physic of the melting process, four videos were collected with a Nikon D610 camera equipped with a 24 mm lens at 60 fps. Fig. 5 reports some peculiar frames of the videos collected during the 20 W tests, the full videos are also available as supplementary data. In particular, Fig. 5a, 5b, 5c, and 5d report the reference, 40 mm, 20 mm, and 10 mm samples images respectively.

All the videos are recorded without thermocouples inserted in the PCM to allow for a clearer visualization of the process. The only thin wire, when present, is the t11 thermocouple wire that was glued on the top of the aluminum structure.

The first frame showed in Fig. 5 is taken when the first melted phase is visible. It appears sooner in the 10 mm sample (after 9 min, Fig. 5d), while later in the reference sample (25 min, Fig. 5a). Since all the specimens were receiving the same amount of heat from the cartridge heater, it can be concluded that the 10 mm sample is able to transfer quicker and more efficiently the heat from the bottom to the top paraffin. In fact, in the 10 mm structure, a higher number of aluminum ligaments (i.e. higher heat transfer area) contribute to spread the electrical heat.

Furthermore, also the distribution of melted and non-melted areas varies among the samples. In the reference one (Fig. 5a), the PCM receives heat from the base and from the lateral aluminum

Fig. 5. a Peculiar frames of the reference sample charging at 20 W video. Fig. 5b. Peculiar frames of the 40 mm sample charging at 20 W video. Fig. 5c. Peculiar frames of the 20 mm sample charging at 20 W video. Fig. 5d. Peculiar frames of the 10 mm sample charging at 20 W video.

Fig. 5 Continued.

walls. Accordingly, it melts starting from the lateral walls and from the bottom. In fact, after about 34 min, a large iceberg-like PCM solid portion is randomly moving in the liquid paraffin wax, like an ice cube in a water glass. Finally, this small PCM volume sinks and, when touching the hot basement, it quickly melts disappearing.

A similar behavior can be identified also in the case of the 40 mm sample (Fig. 5b). In fact, the specimen presents just few thick ligaments that convey the heat inside the PCM. Here the paraffin wax receives the heat from the bottom and the lateral walls, but it can clearly be seen that it is heated also by the central ligaments (for instance, see frame at 16 min). In this case, the 3D structure sticks the solid core, which cannot float on the melted PCM. Hence, the solid PCM remains connected only to the inside ligaments surrounded by the superheated liquid, which has a very low thermal conductivity.

Considering smaller base cell sizes, 20 mm and, especially, 10 mm samples (Fig. 5c and 5d respectively) present a different melting process. Once again, the first melted PCM is visible close to the external walls, and very likely, to the bottom. However, the higher number of ligaments efficiently spread the heat throughout the PCM, allowing for a more uniform temperature distribution and thus phase change process. The last volume to melt is the top layer, which makes the visualization of the process difficult by only means of a camera installed on the top of the sample.

For this reason, the analysis of the measurements of the thermocouples inserted inside the PCM becomes fundamental to better understand the melting process.

Fig. 6 presents the temperature field in the four PCM samples when heated at 20 W. More in detail, Fig. 6a, 6b, 6c, and 6d reports the data collected in the reference, 40 mm, 20 mm, and 10 mm samples, respectively.

At a first glance, the temperatures in the reference and in the 40 mm samples are more scattered as compared to those recorded for 10 mm and 20 mm samples, which means that there is a remarkable difference between the junction ($t3$) temperature and the minimum temperature measured inside the PCM. In the case of the reference sample, the maximum temperature difference reaches more than 40 K, while for the 40 mm sample, it is slightly lower but still around 30 K. For the other two samples, the maximum temperature difference is always lower.

As expected, the junction temperature ($t3$) is always the highest recorded temperature, while the temperatures close to the external walls ($t4$ and $t5$) and to the bottom wall ($t6$) increase quickly, especially in the reference sample and the profiles follow that measured by the $t6$, which is close to the heated surface. This confirms the visual observations discussed before for the reference sample: the paraffin wax melts from the bottom and from the lateral walls and the liquid superheats due to the low thermal conductivity of the
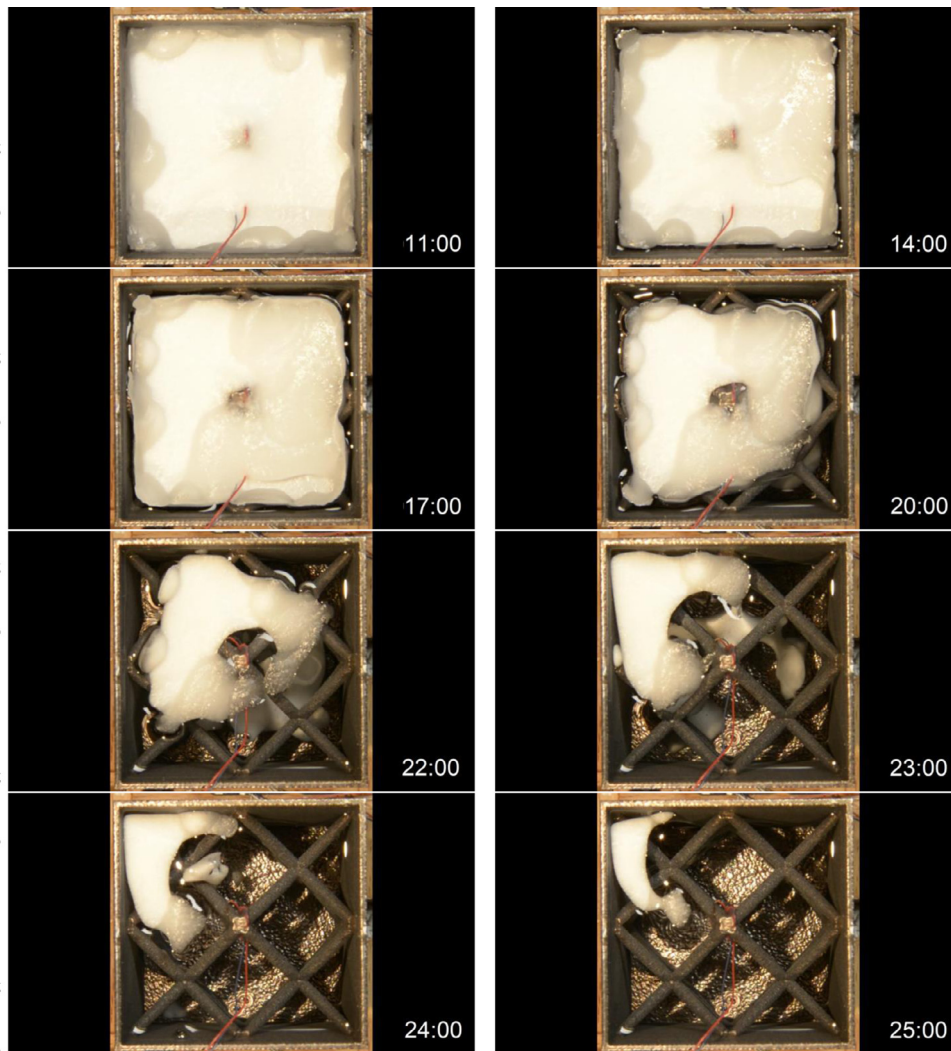
Fig. 5 Continued.

PCM. The solid PCM remains colder and the melting process is very slow. When the 3D periodic structure is added, the behavior recorded by these three thermocouples is different; for instance, in the case of the 40 mm sample, the bottom temperature (t6) and the corner one (t4) increase very fast while the lateral temperature (t5) presents a different profile. In this case (40 mm sample), the thick ligament which originates from the corner heats up quickly the area where t4 is positioned while the thinner walls show a delayed warm up. A similar behavior can be noticed also in the case of 20 mm sample while the temperature profiles of the 10 mm one show that the melting process proceeds from the bottom to the top.

It is also interesting to discuss the behavior showed by t6, which again confirms the behavior highlighted by the visualizations in the case of the reference and 40 mm samples. At the end of the melting process, this thermocouple, which is located 1 mm far from the base, presents a sudden reduction, because the last small piece of relatively cold, solid PCM sinks and reaches the bottom before melting.

In the case of reference, 40 mm and 20 mm samples, the temperature in the center (t8) remains remarkably low for a long part of the test and then quickly increases, defining the moment when the solid core collapses.

As also comes out from the visualizations, the 10 mm sample exhibits a completely different melting process; in fact, no solid core appears and sinks at the end of the test. From the analysis of the temperature distribution, as already stated, the process appears to be developed from the bottom to the top. Hence, t8 gradually increases and the last thermocouple that reaches the melting point is the t9, the temperature on the top PCM layer, which shows the conclusion of the phase change. Again, this means that the last solid PCM remains in the top layer, as observed in the video recorded and previously commented in the same paragraph.

Particular attention should be given to the junction temperature. This value is rather meaningful since it represents the temperature of a potential electronic device during functioning when coupled to a PCM heat storage.

Table 4 summarizes the junction temperature (t3) at the end of the melting phase and the temperature reduction obtained with the 3D structures with respect to the reference.

The highest junction temperature is always reached when the reference sample is used. In this case, no additional structures help to spread the heat. The highest reductions are exhibited by the 10 mm sample at 30 W, which reaches −18.6 K. However, especially at 10 and 20 W there is not any appreciable difference among the performance of the three periodic structures in terms of maximum junction temperature

To further analyze and confirm the previous considerations, it is possible to study the temperature of the central top aluminum ligament (t11). The values of the maximum temperature reached by t11 at the end of the charging phase are listed in Table 5 for all the 3D structures (obviously it is not present in the reference sample).
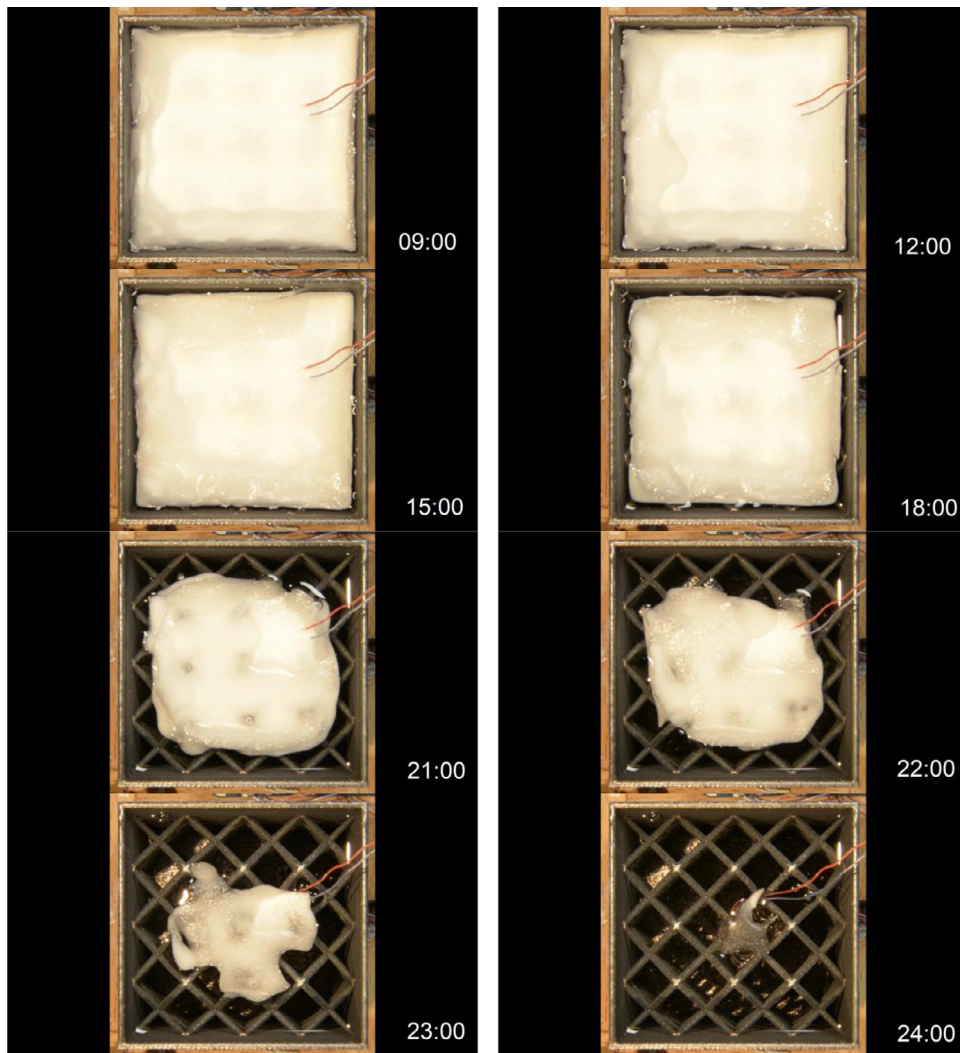
Fig. 5 Continued.

Discharging phase

The discharging phase can be studied in terms of time of solidifi-cation from the end of the melting (i.e., when the cartridge heater is switched off) and the moment in which the PCM reaches a specific temperature. In the present work, two discharging times are defined. The first, named total discharging time, is defined as the time needed by the entire PCM to reach a temperature below 25 °C. The second, named partial discharging time, refers to the time needed by the PCM to reach a temperature 10 K lower than the phase change tem-perature (i.e., 60 °C). During the discharging phase, the samples exchange heat in natural convection with the surroundings, being located in a climatic chamber set at 20 °C.

Table 6 resumes the total and the partial discharging times and the corresponding percentage time reduction with respect to the ref-erence sample collected after the three different charging phases at: 10, 20, and 30 W. It has to be pointed out that, as reported in Table 4, the samples reached different temperatures at the end of the

The 10 mm specimen presents a t11 temperature always lower than the other structures, implying a more efficient heat transfer in the lower regions of the container. Oppositely, in the 40 mm sample, the heat seems to move faster to the upper region through the fewer but thicker ligaments.

charging phases run at different imposed heat flux, hence, the dis-charging phases start at different initial temperatures.

The longest discharging times are recorded for the reference sam-ple after the 30 W charging test. This result was expectable, since the reference sample does not present any aluminum structure that can help in spreading the heat through the PCM and because the 30 W heating phase leads to the highest temperatures in the PCM. In any case, the discharging times measured for both the reference and the 3D periodic structures samples are much longer than the charging ones. This can be explained considering that during the discharging phase the heat is exchanged mainly by natural convection through the aluminum lateral walls and it decreases as the wall temperature decreases. It can be stated that the latent heat storage working cycle is much more affected by the discharging phase. For these reasons, it would be interesting in a future research enhancing the cooling down efficiency with the aim of reaching similar charging and dis-charging times.

In general, it can be stated that the 10 mm sample exhibits the best performance showing consistent time reductions, which on average are more than 20% when considering 25 °C as final tempera-ture while it is more than 40% for the 60 °C. Then, the improvement of the discharging phase worsens as the base size decreases.

Fig. 7 reports the temperature in the middle of the PCM samples (t8) during the discharging phase after a charging carried out at 30 W (a), 20 W (b), and 10 W (c), respectively.
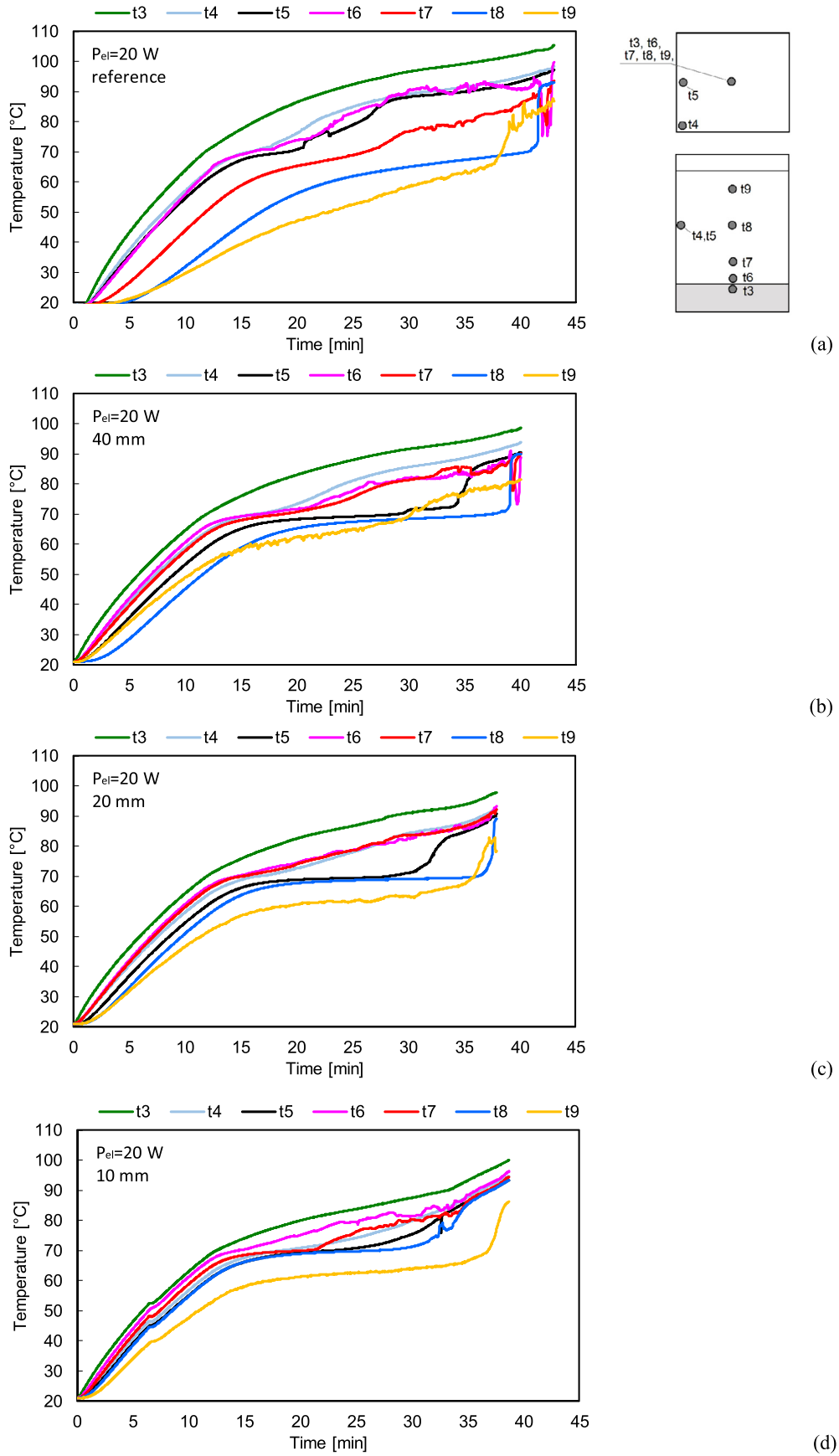
Fig. 6. RT70 charging phase at 20 W in the reference, 40 mm, 20 mm, and 10 mm samples.

At all the investigated imposed heat fluxes, the reference sample reaches higher final temperatures during the charging phase, in fact it requires a longer time to completely melt the PCM due to a less efficient heat spreading capability. For this reason, the liquid superheats and, consequently, the maximum temperature increases. Thus, the discharging phase starts at higher temperatures and it takes a great amount of sensible heat to be rejected to de-superheat the liquid, which leads to longer times. In general, the de-superheating and the subcooling profiles present almost similar slopes for all the tested samples.

Considering the data relative to 30 W and 20 W, the phase change interval (i.e., when the temperature is almost constant) is much longer for the reference sample as compared to the other ones. When the periodic structures are used, the heat transfer performance improves and the enhancement increases as the base size decreases.

Fig. 8 shows a few interesting frames of the video recorded during the discharging phase for the four tested samples (the full videos are available as supplementary data). Differently to what has been done during the charging phase, in order to have a direct and fair comparison of the discharging phase of all the samples, it was decided to heat the specimens inside an oven up to 75 °C. When all the paraffin wax masses contained in each specimen were totally melted and reached the oven temperature, the samples were located in the 20 °C climatic room and the video was recorded. Of course, this test differs from the discharging ones collected during the experimental campaign but it allows for a direct visual comparison between the samples giving new insight on the underlining heat transfer mechanisms on the basis of the solidification process inside 3D periodic structures.

As described in Fig. 8, the reference structure is located top right, the 40 mm one top left, the 20 mm bottom left and the 10 mm bottom right.

At the beginning of the test (frame 0 min) all the wax was liquid. Just 1 min after, it is possible to detect a very thin solid layer on the top of the liquid in the 10 mm and the 20 mm samples, and few solidified spots on the 40 mm top. After about 2 min the solid layer appears also on the top of the reference sample, and then after 3 min, all the samples are covered by a thin layer of solid PCM and the solidification process continues towards the inside. Thus, in the subsequent minutes, the solid layer thickens and it does not permit to see inside anymore.

Fig. 9 presents the temperature recorded by the thermocouples inserted in the reference (a), 40 mm (b), 20 mm (c) and in the 10 mm (d) samples during the discharging phase after a 20 W heating.

Similarly, to what it happens in the charging phase, the temperature field is more scattered in the reference specimen, while the 3D structures tend to homogenize the temperature. The smaller the base size, the more homogeneous the temperature. In fact, the best performance is exhibited by the 10 mm sample in which, apart from the very top thermocouple (t9) which cools down very fast, all the other temperatures show very similar profiles meaning that the

Table 4
Maximum junction temperature (t3) reached at the end of the melting phase and percentage time reduction with respect to the reference.

| T max junction (°C) | | | | |
	Reference	40 mm	20mm	10 mm
10 W	89.8	86.2	86.4	86.0
20 W	107.6	98.9	98.0	100.5
30 W	125.6	111.8	108.1	107

| Reduction with respect to the reference (K) | | | | |
	Reference	40 mm	20mm	10 mm
10 W	–	−3.6	−3.4	−3.8
20 W	–	−8.7	−9.6	−7.1
30 W	–	−13.8	−17.5	−18.6

Table 5
Maximum temperature reached by t11 at the end of the charging phase.

t11	Reference	10 mm	20mm	40 mm
10 W	–	81.2	82.8	82.8
20 W	–	88.2	91.6	95.5
30 W	–	99.2	101.3	100.6

solidification occurs uniformly inside the PCM. In the case of the reference sample, the max-min temperature difference reaches almost 30 K, and the last zone that solidifies is the center (t8).

These experimental results confirm the phenomenology described by means of the frames extracted by the video and reported in Fig. 8.

PCMs comparison

This section reports a brief comparison of the phase change behavior of the RT70 and of RT55, which presents a different melting temperatures (i.e. around 55 °C). The results here proposed are partially reported in Righetti et al. [18] and they were run following the same experimental procedure used in the present work. This comparison permits to highlight the peculiar heat transfer properties and of the two paraffin waxes, which apart from the latent heat of fusion (260 kJ kg^{-1} for the RT70 and 180 kJ kg^{-1} for the RT55), show similar thermo-physical properties.

A PCM with a relatively high melting temperature, like RT70, forces the system to work at a consequently high temperature interval, differently, if a lower phase change temperature PCM is used, a lower working temperature could be reached.

Fig. 10 presents the comparison between RT70 and RT55 during the charging at 20 W (a) and the consequent discharging (b) in the 10 mm sample. The y-axis reports the temperature difference defined as the average PCM temperature (i.e. the average value of t4, t5, t, t7,

Table 6
Discharging times up to 25 °C and up to 60 °C and corresponding percentage time reduction with respect to the reference sample.

| Discharging times up to 25 °C (min) | | | | |
	Reference	40 mm	20mm	10 mm
10 W	194	182	162	146
20 W	194	172	154	157
30 W	215	189	160	159

| Discharging times up to 60 °C (min) | | | | |
	Reference	40 mm	20mm	10 mm
10 W	98	75	60	54
20 W	103	83	59	63
30 W	110	85	72	65

| Percentage reduction with respect to the reference (%) Discharging times up to 25 °C | | | | |
	Reference	40 mm	20mm	10 mm
10 W	–	−6.2	−16.5	−24.7
20 W	–	−11.3	−20.6	−19.1
30 W	–	−12.1	−25.6	−26

| Discharging times up to 60 °C | | | | |
	Reference	40 mm	20mm	10 mm
10 W	–	−23.5	−38.8	−44.9
20 W	–	−19.4	−42.7	−38.8
30 W	–	−22.7	−34.5	−40.9
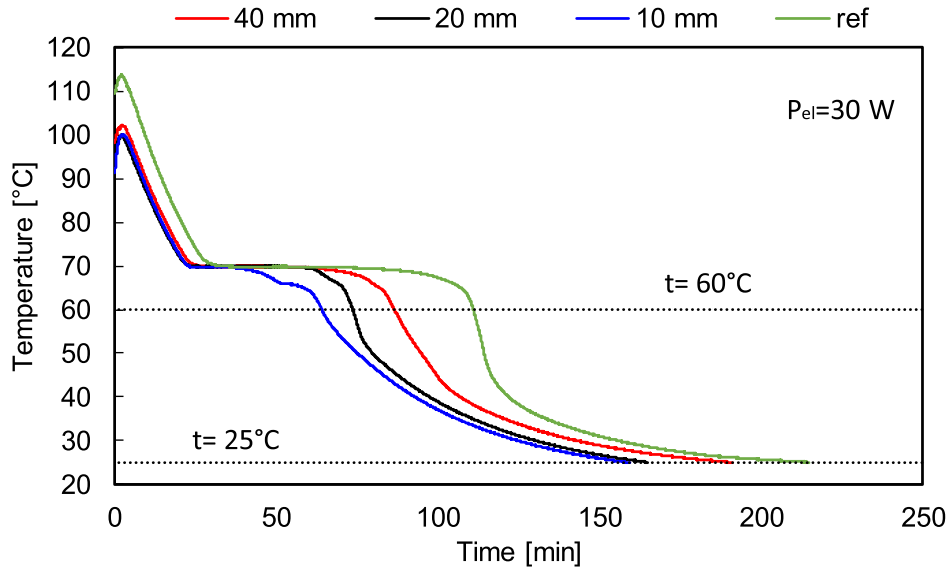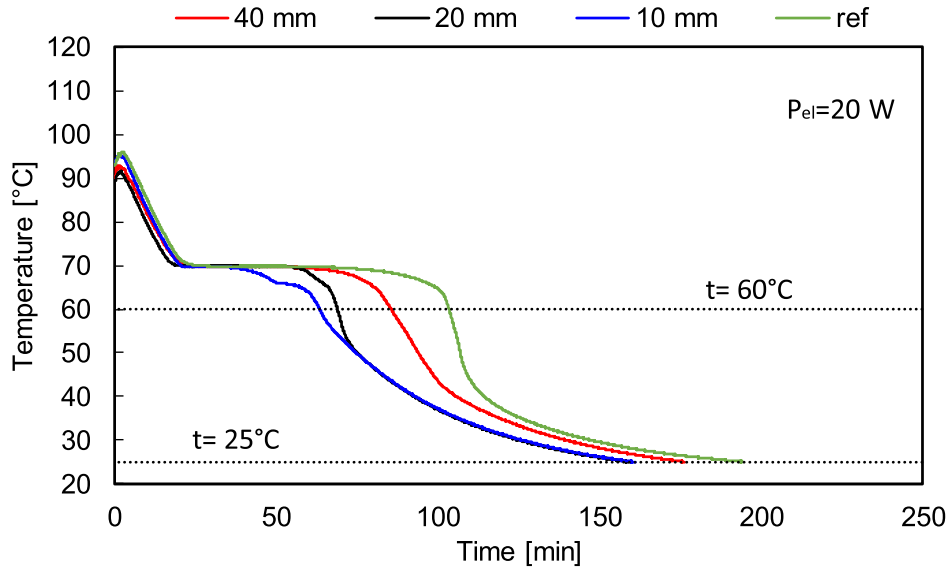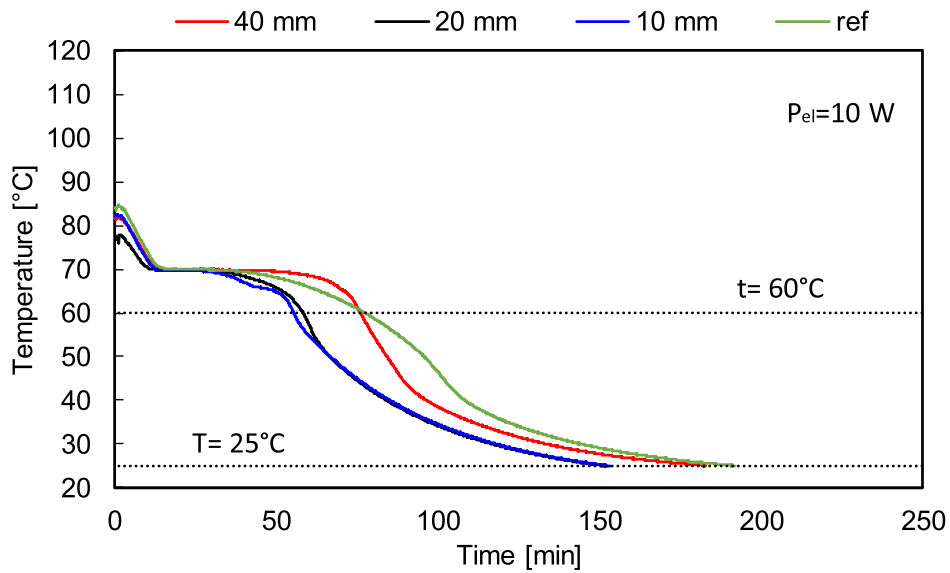
Fig. 7. t8 temperature, in the middle of the 40, 20, 10 mm samples and the reference one during RT70 discharging phase after a charging phase carried out at 30, 20, and 10 W.
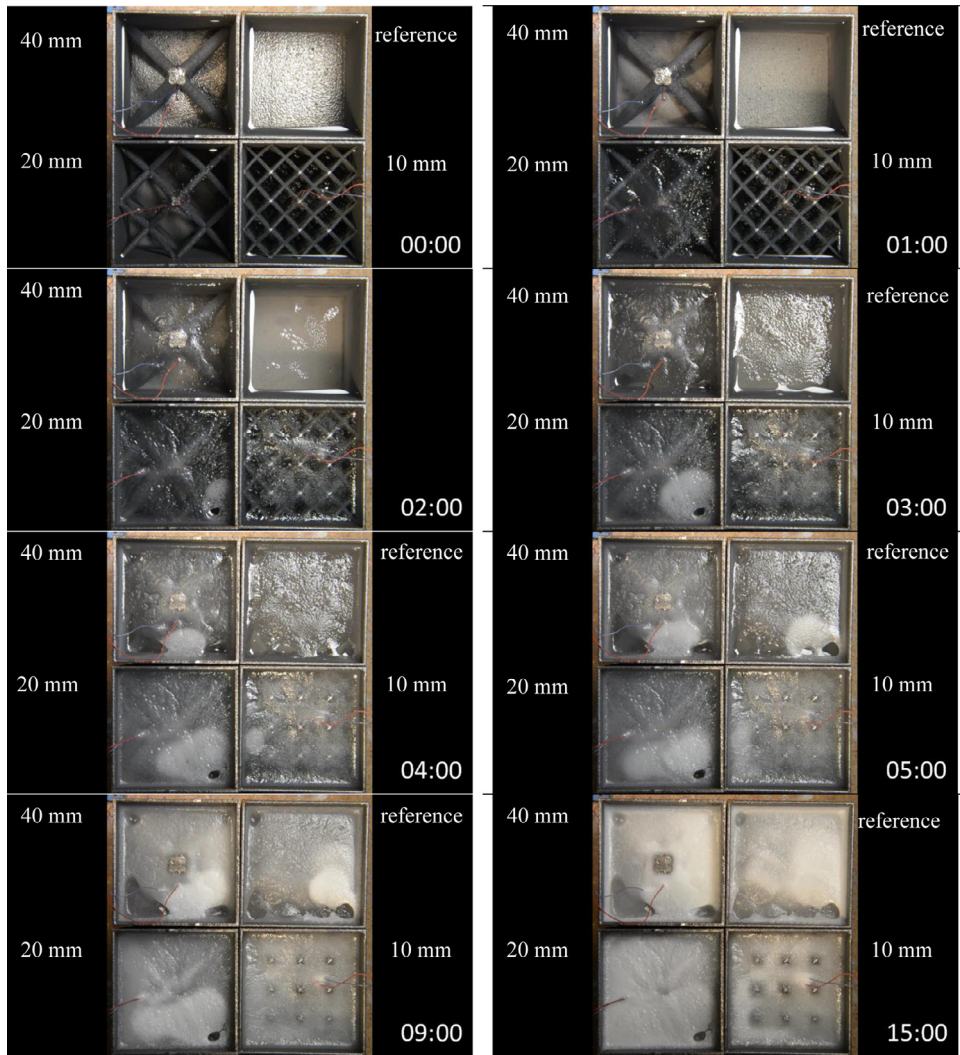
Fig. 8. Relevant frames of the discharging process staring with all the samples initial bulk temperature of 70 °C.

t8, and t9) minus the nominal melting temperature (i.e. 70 °C for RT70 and 55 °C for RT55).

By comparing the data plotted in the diagrams, it clearly appears that the slopes of the temperature difference profiles of the two paraffin waxes during the sensible heating and de-superheating are almost similar; this result confirms that the two PCM have almost the same thermal conductivity in both solid and liquid phases.

Considering the charging phase (Fig. 10a), being the heat flux kept constant, the RT55 exhibits a faster process since it has a lower latent heat and it has to reach a lower final temperature.

Differently, during the discharging phase, the two paraffin waxes exhibit similar solidification times despite that their latent heat are different and, furthermore, in the case of the RT70, also the driving cooling temperature difference between wax and air is much higher.

Non-dimensional modeling

The collected experimental data were then used to validate a semi-empirical correlation to estimate the junction temperature, a very important parameter to control when such latent heat thermal energy storages are used. This correlation was proposed by Righetti et al. [18], who modified the model initially developed by Mallow et al. [10], and also implemented by Diani and Campanale [2] in the particular case of PCM embedded in metal foams. The correlation is based on a non-dimensional analysis that takes into account the main thermophysical properties of the composite material.

This composite material is a fictitious material that includes both the PCM and the 3D periodic metallic structure.

According to Mallow et al. [10], the density, the thermal conductivity, the specific heat, and the latent heat of the composite material can be evaluated as Eqs. (4), 5, 6, and 7 respectively:

$$\rho_{COM} = \varepsilon \cdot \rho_{PCM} + (1-\varepsilon) \cdot \rho_s \tag{3}$$

$$\lambda_{COM} = 0.33 \cdot \lambda_s \cdot (1-\varepsilon) \tag{4}$$

$$c_{p,COM} = \varepsilon \cdot \frac{\rho_{PCM}}{\rho_{COM}} \cdot c_{p,PCM} + (1-\varepsilon) \cdot \frac{\rho_s}{\rho_{COM}} c_{p,s} \tag{5}$$

$$r_{COM} = \varepsilon \cdot \frac{\rho_{PCM}}{\rho_{COM}} \cdot r_{PCM} \tag{6}$$

The porosity ε of the present specimens is 0.95, and the thermal conductivity of the AlSi10Mg-0403 aluminum alloy once printed was measured to be equal to $\lambda_s = 96 \, W \, m^{-1} \, K^{-1}$. The aluminum density was set at 2700 kg m^{-3}, as declared by the manufacturer, while the specific heat equal to 800 J kg^{-1} K^{-1}.

Table 7 resumes the values of the main thermophysical properties at 20 °C of the composite material composed by RT70 and the investigated 3D printed aluminum specimens.

As proposed by Righetti et al. [18], the correlation is based on three non-dimensional parameters: the modified Stefan number Ste, the Fourier number Fo, and the non-dimensional temperature θ,
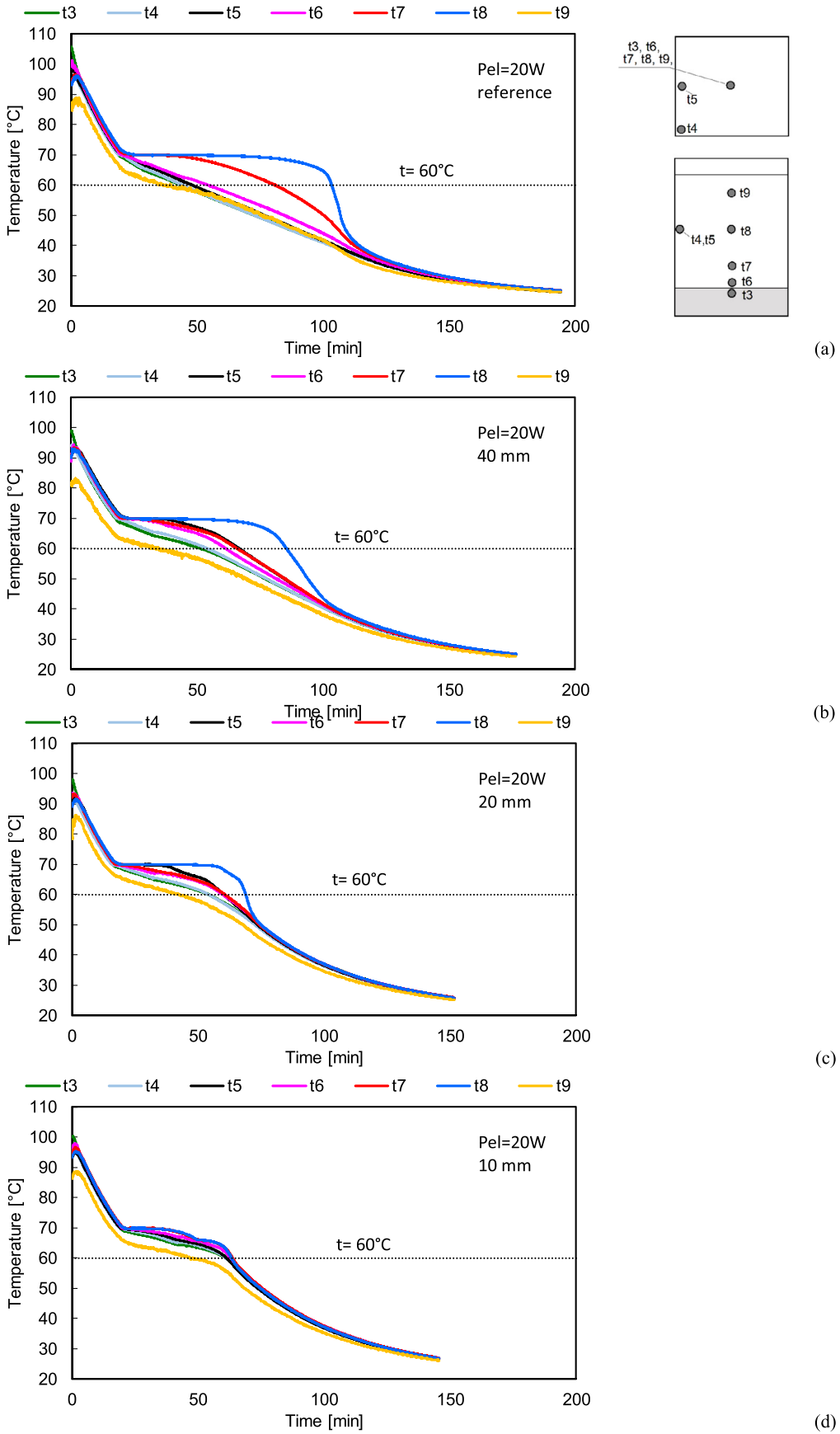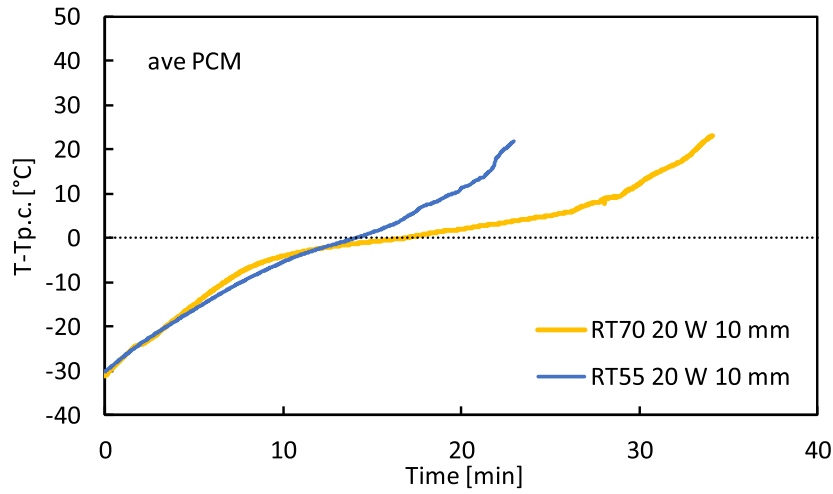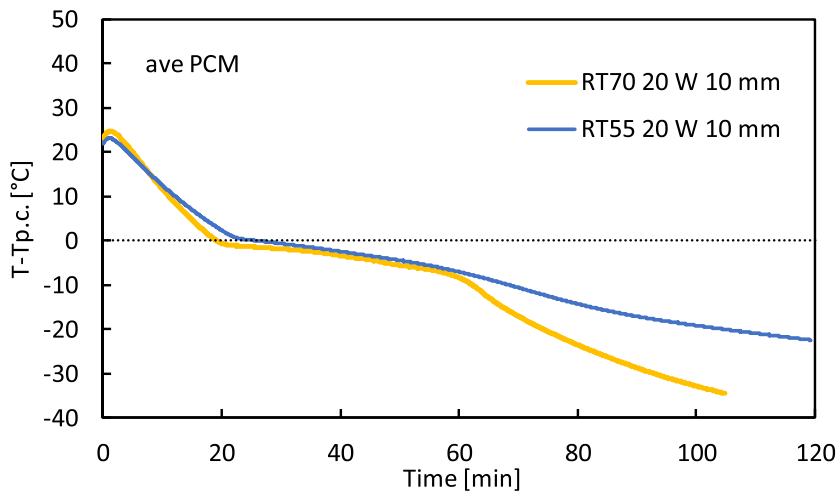
Fig. 9. Temperature recorded by the thermocouples inserted in the reference, 40, 20 and in the 10 mm samples during the discharging phase after a 20 W heating.

(a)

(b)

Fig. 10. Comparison between RT70 and RT55 paraffin waxes during charging at 20 W (a) and discharging after a 20 W heating (b) in the 10 mm sample.

defined as following by Eqs. (8), 9, and 10 respectively:

$$\text{Ste} = \frac{c_{p,COM} \cdot (T_{melt} - T_i)}{r_{COM} + c_{p,COM} \cdot (T_{melt} - T_i)} \tag{7}$$

$$\text{Fo} = \frac{\lambda_{COM} \cdot \tau_{melt}}{\rho_{COM} \cdot h^2 \cdot c_{p,COM}} \tag{8}$$

$$\Theta = \frac{T_j - T_{melt}}{T_{melt} - T_i} \tag{9}$$

The resulting equation from the experimental data collected and here proposed is:

$$\Theta = 0.31 \cdot (\text{Ste} \cdot \text{Fo})^{-0.69} \tag{10}$$

Table 7
thermophysical properties at 20 °C of the composite material.

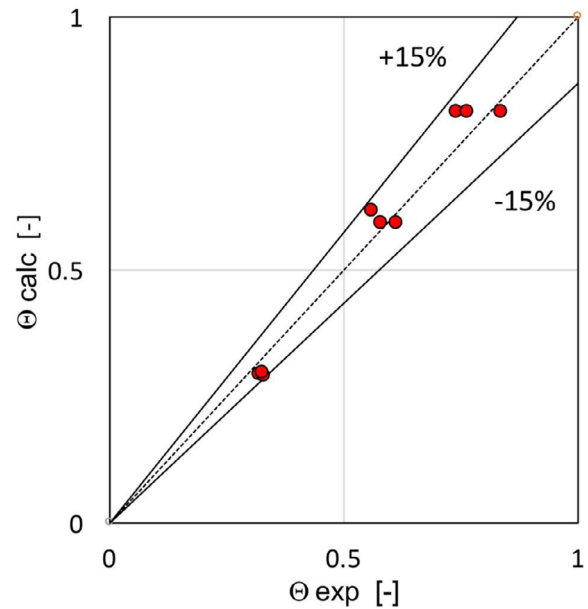| Property	Calculated value
λ_{COM}	1.584 W $m^{-1} K^{-1}$
ρ_{COM}	971 kg m^{-3}
$c_{p,COM}$	1847 J $kg^{-1} K^{-1}$
r_{COM}	223.85 kJ kg^{-1}

Fig. 11. Experimental vs. calculated non-dimensional temperature evaluated by using the here proposed correlation.

This correlation is able to predict the experimental data with a mean relative deviation of −0.7%, an mean absolute deviation of 7.0% and a standard deviation of 8.1%. Fig. 11 presents the comparison between experimental and calculated non-dimensional junction temperature, the model shows a very good agreement also with the present experimental data.

Conclusions

A paraffin wax with a phase change temperature of 70 °C was selected as PCM to be implemented in LTESs. Three aluminum 3D periodic structures were designed, 3D printed and then studied to enhance the heat transfer performance of the paraffin wax. They all presented the same porosity to investigate the effect of the cell base size. All the structures were heated with a constant heat flux from the bottom generated by a cartridge heater and then were cooled down by still ambient air at 20 °C. The charging (from ambient air to the total melt) and the discharging (from the switch-off of the electrical heater to 25 °C) phases were studied by imposing three different heat fluxes (10, 20, and 30 W).

The 3D periodic structures remarkably enhance the heat transfer performance of the LTES, in fact, in all cases the charging and discharging time are reduced.

This can be explained considering that the aluminum ligaments of the 3D periodic structures increase the heat transfer area, since they are directly connected to the heated basement, and thus they improve the heat spreading throughout the paraffin.

Among the three structures, the most efficient is revealed to be the 10 mm one, which allows for more significant time reductions than the others during both the charging and discharging phases (up to 17% during charging and up to 26% during discharging). Since the time reduction increases with the decreasing of the base size, a sample having an even smaller base size (for instance 5 mm or so) might be even more efficient than the 10 mm.

The melting process was studied by collecting some videos and by analyzing the temperature field inside the PCM: the 10 mm structure presented a different melting behavior thanks to the higher number of ligaments that spread the heat inside the PCM.

The discharging time is much longer than the charging one. So, the working cycle is much more affected by the discharging phase. This opens new interesting research opportunity to investigate how to reduce the overall thermal resistance of the system that during the discharging phase is dominated by natural convection through the walls rather than by the internal heat conduction inside the PCM.

Finally, a correlation recently proposed by Righetti et al. [18] to evaluate the junction temperature in a latent heat storage where a PCM is coupled with a 3D periodic structure is validated against the new present experimental database. The correlation was able to fairly predict the experimental data with a relative deviation of −0.7%, an absolute deviation of 7.0% and a standard deviation of 8.1%.

Declaration of Competing Interest

The authors declare that they have no known competing financial interests or personal relationships that could have appeared to influence the work reported in this paper.

Supplementary materials

Supplementary material associated with this article can be found, in the online version, at doi:10.1016/j.ijft.2020.100035.

References

[1] M. Al-Maghalseh, M., K. Mahkamov, Methods of heat transfer intensification in PCM thermal storage systems: Review paper, Renew. Sust. Energ. Rev 92 (2018) 62–94 https://doi.org/, doi: 10.1016/j.rser.2018.04.064.

[2] A. Diani, M. Campanale, Transient melting of paraffin waxes embedded in aluminum foams: Experimental results and modeling, Int. J. Therm. Sci. 144 (2019) 119–128 https://doi.org/, doi: 10.1016/j.ijthermalsci.2019.06.004.

[3] S.F. Hosseinizadeh, F.L. Tan, S.M. Moosania, Experimental and numerical studies on performance of PCM-based heat sink with different configurations of internal fins, Appl. Therm. Eng. 31 (2011) 3827–3838 https://doi.org/, doi: 10.1016/j.applthermaleng.2011.07.031.

[4] K.A.R. Ismail, F.A.M. Lino, Fins and turbulence promoters for heat transfer enhancement in latent heat storage systems, Exp. Therm. Fluid Sci. 35 (2011) (2011) 1010–1018 https://doi:, doi: 10.1016/j.expthermflusci.2011.02.002.

[5] L. Kalapala, J.K. Devanuri, Influence of operational and design parameters on the performance of a PCM based heat exchanger for thermal energy storage, A review Journal of Energy Storage 20 (2018) 497–519 https://doi.org/, doi: 10.1016/j.est.2018.10.024.

[6] B. Kamkari, D. Groulx, Experimental investigation of melting behavior of phase change material in finned rectangular enclosures under different inclination angles, Exp. Therm. Fluid Sci. 97 (2018) 94–108 https://doi.org/, doi: 10.1016/j.expthermflusci.2018.04.007.

[7] Z. Khan, Z. Khan, A. Ghafoor, A review of performance enhancement of PCM based latent heat storage system within the context of materials, thermal stability and compatibility, Energy Conversion and Management 115 (2016) 132–158 http://dx.doi.org/, doi: 10.1016/j.enconman.2016.02.045.

[8] J.M. Mahdi, S. Lohrasbi, E.C. Nsofor, Hybrid heat transfer enhancement for latent-heat thermal energy storage systems: A review, Int. J. Heat Mass Transf. 137 (2019) 630–649 https://doi.org/, doi: 10.1016/j.ijheatmasstransfer.2019.03.111.

[9] S. Mahmoud, A. Tang, C. Toh, R. Al-Dadah, S.L. Soo, Experimental investigation of inserts configurations and PCM type on the thermal performance of PCM based heat sinks, Appl. Energ. 112 (2013) 1349–1356 https://doi.org/, doi: 10.1016/j.apenergy.2013.04.059.

[10] A. Mallow, O. Abdelaziz, S. Graham, Thermal charging performance of enhanced phase change material composites for thermal battery design, Int. J. Therm. Sci. 27 (2018) 19–28 https://doi.org/, doi: 10.1016/j.ijthermalsci.2017.12.027.

[11] S. Mancin, A. Diani, L. Doretti, K. Hooman, L. Rossetto, Experimental analysis of phase change phenomenon of paraffin waxes embedded in copper foams, Int. J. Therm. Sci. 90 (2015) 79–89 https://doi.org/, doi: 10.1016/j.ijthermalsci.2014.11.023.

[12] A. Mustaffar, A. Harvey, D. Reay, Melting of phase change material assisted by expanded metal mesh, Appl. Therm. Eng. 90 (2015) 1052–1060 https://doi.org/, doi: 10.1016/j.applthermaleng.2015.04.057.

[13] G. Patankar, S. Mancin, J.A. Weibel, S.V. Garimella, M.A. McDonald, A Method for Thermal Performance Characterization of Ultra-Thin Vapor Chambers Cooled by Natural Convection, ASME. J. Electron. Packag. 138 (1) (2016) 010,903.

[14] P. Ping, R. Peng, D. Kong, G. Chen, J. Wen, Investigation on thermal management performance of PCM-fin structure for Li-ion battery module in high-temperature environment, Energy conversion and management 176 (2018) 131–146 https://doi.org/, doi: 10.1016/j.enconman.2018.09.025.

[15] K.S. Reddy, V. Mudgal, T.K. Mallick, Review of latent heat thermal energy storage for improved material stability and effective load management, Journal of Energy Storage 15 (2018) 205–227 https://doi.org/, doi: 10.1016/j.est.2017.11.005.

[16] T. Rehman, H.M. Ali, M.M. Janjua, U. Sajjad, W.M. Yan, A critical review on heat transfer augmentation of phase change materials embedded with porous materials/foams, Int. J. Heat Mass Transf. 135 (2019) 649–673 https://doi.org/, doi: 10.1016/j.ijheatmasstransfer.2019.02.001.

[17] G. Righetti, R. Lazzarin, M. Noro, S. Mancin, Phase Change Materials embedded in porous matrices for hybrid thermal energy storages: experimental results and modeling, Int. J. Refrig 106 (2019) 266–277 https://doi.org/, doi: 10.1016/j.ijrefrig.2019.06.018.

[18] G. Righetti, G. Savio, R. Meneghello, L. Doretti, S. Mancin, Experimental study of phase change material (PCM) embedded in 3D periodic structures realized via additive manufacturing, International Journal of Thermal Sciences 153 (2020) July 2020, 106,376, https://doi.org/, doi: 10.1016/j.ijthermalsci.2020.106376.

[19] S.Z. Shuja, B.S. Yilbas, M.M. Shaukat, Melting enhancement of a phase change material with presence of a metallic mesh, Appl. Therm. Eng. 79 (2015) 163–173 http://dx.doi.org/, doi: 10.1016/j.applthermaleng.2015.01.033.

[20] Z. Sun, R. Fan, F. Yan, T. Zhou, N. Zheng, Thermal management of the lithium-ion battery by the composite PCM-Fin structures, International Journal of Heat and Mass Transfer 145 (2019) 118 739 https://doi.org/, doi: 10.1016/j.ijheatmasstransfer.2019.118739.

[21] Y.B. Tao, Y.L. He, A review of phase change material and performance enhancement method for latent heat storage system, Renewable and Sustainable Energy Reviews 83 (2018) 245–259 https://doi.org/, doi: 10.1016/j.rser.2018.05.028.

[22] A. Verma, S. Shashidhara, D. Rakshit, A comparative study on battery thermal management using phase change material (PCM), Thermal Science and Engineering Progress 11 (2019) 74–83 https://doi.org/, doi: 10.1016/j.tsep.2019.03.003.

[23] J. Weng, Y. He, D. Ouyang, X. Yang, G. Zhang, J. Wan, Thermal performance of PCM and branch-structured fins for cylindrical power battery in a high-temperature environment, Energy Conversion and Management 200 (2019) 112 106 https://doi.org/, doi: 10.1016/j.enconman.2019.112106.

[24] Z. Zhou, Z. Zhang, J. Zuo, K. Huang, L. Zhang, Phase change materials for solar thermal energy storage in residential buildings in cold climate, Renew. Sust. Energ. Rev. 48 (2015) 692–703 http://dx.doi.org/, doi: 10.1016/j.rser.2015.04.0481364−0321.